Quantum control study of ultrafast optical responses in semiconductor quantum dot devices

Jung Y. Huang, [1,*] **Chien Y. Lin,** [1] **Wei-Sheng Liu,** [2] **and Jen-Inn Chyi**[2]

[1] *Department of Photonics, Chiao Tung University, Hsinchu, Taiwan*
[2] *Department of Electrical Engineering, Central University, Chung-Li 320, Taiwan*
[*] *jyhuang@faculty.nctu.edu.tw*

Abstract: Two quantum control spectroscopic techniques were applied to study InAs quantum dot (QD) devices, which contain different strain-reducing layers. By adaptively control light matter interaction, a delayed resonant response from the InAs QDs was found to be encoded into the optimal phase profile of ultrafast optical pulse used. We verified the delayed resonant response to originate from excitons coupled to acoustic phonons of InAs QDs with two-dimensional coherent spectroscopy. Our study yields valuable dynamical information that can deepen our understanding of the coherent coupling process of exciton in the quantum-confined systems.

OCIS codes: (230.5590) Quantum dots; (320.5540) Pulse shaping; (320.7090) Ultrafast lasers; (190.7110) Ultrafast nonlinear optics; (300.6530) Ultrafast Spectroscopy.

References and links

1. D. Bimberg, M. Grundmann, and N. N. Ledentsov, *Quantum Dot Heterostructures* (Wiley, 1998).
2. P. C. Chiu, W. S. Liu, M. J. Shiau, J. I. Chyi, W. Y. Chen, H. S. Chang, and T. M. Hsu, "Enhancing the optical properties of InAs quantum dots by an InAlAsSb overgrown layer," Appl. Phys. Lett. **91**, 153106 (2007).
3. W. S. Liu, H. L. Tseng, and P. C. Kuo, "Enhancing optical characteristics of InAs/InGaAsSb quantum dot structures with long-excited state emission at 1.31 um," Opt. Express **22**(16), 18860–18869 (2014).
4. Y. Arakawa and H. Sakaki, "Multidimensional quantum well laser and temperature dependence of its threshold current," Appl. Phys. Lett. **40**(11), 939–941 (1982).
5. D. L. Huffaker, G. Park, Z. Zou, O. B. Shchekin, and D. G. Deppe, "1.3 um room-temperature GaAs-based quantum-dot laser," Appl. Phys. Lett. **73**(18), 2564–2566 (1998).
6. K. Mukai, Y. Nakata, K. Otsubo, M. Sugawara, N. Yokoyama, and H. Ishikawa, "1.3-um CW lasing of InGaAs-GaAs quantum dots at room temperature with a threshold current of 8 mA," IEEE Photon. Technol. Lett. **11**(10), 1205–1207 (1999).
7. B. J. Stevens, D. T. D. Childs, H. Shahid, and R. A. Hogg, "Direct modulation of excited state quantum dot lasers," Appl. Phys. Lett. **95**(6), 061101 (2009).
8. C. S. Lee, P. Bhattacharya, T. Frost, and W. Guo, "Characteristics of a high speed 1.22um tunnel injection p-doped quantum dot excited state laser," Appl. Phys. Lett. **98**(1), 011103 (2011).
9. W. S. Liu, H. Chang, Y. S. Liu, and J. I. Chyi, "Pinholelike defects in multistack 1.3 um InAs quantum dot laser," J. Appl. Phys. **99**(11), 114514 (2006).
10. J. M. Ripalda, D. Granados, Y. Gonzalez, A. M. Sanchez, S. I. Molina, and J. M. Garcia, "Room temperature emission at 1.6 um from InGaAs quantum dots capped with GaAsSb," Appl. Phys. Lett. **87**(20), 202108 (2005).
11. R. S. Judson and H. Rabitz, "Teaching lasers to control molecules," Phys. Rev. Lett. **68**, 1500–1503 (1992).
12. A. M. Weiner, "Femtosecond pulse shaping using spatial light modulators," Rev. Sci. Instrum. **71**, 1929–1960 (2000).
13. S. S. Szigeti, A. R. Carvalho, J. G. Morley, and M. R. Hush, "Ignorance is bliss: General and robust cancellation of decoherence via no-knowledge quantum feedback," Phys. Rev. Lett. **113**, 020407 (2014).
14. T. C. Weinacht and P. H. Bucksbaum, "Using feedback for coherent control of quantum systems," J. Opt. B Quantum Semiclass. Opt. **4**, R35–R52 (2001).

#222441 - $15.00 USD Received 3 Sep 2014; revised 29 Oct 2014; accepted 21 Nov 2014; published 4 Dec 2014

15. D. J. Tannor and S. A. Rice, "Control of selectivity of chemical reactions via control of wavepacket evolution," J. Chem. Phys. **83**, 5013–5018 (1985).
16. P. Brumer and M. Shapiro, "Control of unimolecular reactions using coherent light," Chem. Phys. Lett. **126**, 541–564 (1986).
17. A. M. Weiner, S. Oudin, D. E. Leaird, and D. H. Reitze, "Shaping of femtosecond pulses using phase-only filters designed by simulated annealing," J. Opt. Soc. Am. A **10**, 1112–1120 (1993).
18. M. A. Montgomery and N. H. Damrauer, "Elucidation of control mechanisms discovered during adaptive manipulation of [Ru(dpb)3](PF6)2 emission in the solution phase," J. Phys. Chem. A **111**, 1426–1433 (2007).
19. D. M. Jonas, "Two-dimensional femtosecond spectroscopy," Annu. Rev. Phys. Chem. **54**, 425–463 (2003).
20. X. Li, T. Zhang, C. N. Borca, and S. T. Cundiff, "Many-Body Interactions in Semiconductors Probed by Optical Two-Dimensional Fourier Transform Spectroscopy," Phys. Rev. Lett. **96**, 057406 (2006).
21. D. B. Turner, P. Wen, D. H. Arias, K. A. Nelson, H. Li, G. Moody, M. E. Siemens, and S. T. Cundiff, "Persistent exciton-type many-body interactions in GaAs quantum wells measured using two-dimensional optical spectroscopy," Phys. Rev. B **85**, 201303(R) (2012).
22. K. W. Stone, K. Gundogdu, D. B. Turner, X. Li, S. T. Cundiff, K. A. Nelson, "Two-Quantum 2D FT Electronic Spectroscopy of Biexcitons in GaAs Quantum Wells," Science **324**, 1169–1173 (2009).
23. E. L. Read, G. S. Engel, T. R. Calhoun, T. Mancal, T. K. Ahn, R. E. Blankenship, and G. R. Fleming, "Cross-peak-specific two-dimensional electronic spectroscopy," Proc. Natl. Acad. Sci. **104**, 14203–14208 (2007).
24. J. O. Tollerud, C. R. Hall, and J. A. Davis, "Isolating quantum coherence using coherent multi-dimensional spectroscopy with spectrally shaped pulses," Opt. Express **22**, 6719–6733 (2014).
25. M. C. Chen, J. Y. Huang, Q. Yang, C. L. Pan, and J. I. Chyi, "Freezing phase scheme for fast adaptive control and its application to characterization of femtosecond coherent optical pulses reflected from semiconductor saturable absorber mirrors," J. Opt. Soc. Am. B **22**, 1134–1121 (2005).
26. M. C. Chen, J. Y. Huang, and L. Chen, "Coherent control multiphoton processes in semiconductor saturable Bragg reflector with freezing phase algorithm," Appl. Phys. B **80**, 333–340 (2005).
27. A. Raisanen, L. J. Brillson, R. S. Goldman, K. L. Kavanagh, and H. H. Wieder, "Optical detection of misfit dislocation-induced deep levels at InGaAs/GaAs heterojunctions," Appl. Phys. Lett. **64**, 3572–3574 (1994).
28. D. Meshulach and Y. Silberberg, "Coherent quantum control of multiphoton transitions by shaped ultrashort optical pulses," Phys. Rev. A **60**, 1287–1292 (1999).
29. S. F. Ren, D. Lu, and G. Qin, "Phonon modes in InAs quantum dots," Phys. Rev. B **63**, 195315 (2001).
30. I. A. Ostapenko, G. Honig, S. Rodt, A. Schliwa, A. Hoffmann, D. Bimberg, M. R. Dachner, M. Richter, A. Knorr, S. Kako, and Y. Arakawa, "Exciton acoustic-phonon coupling in single GaN/AlN quantum dots," Phys. Rev. B **85**, 081303(R) (2012).
31. D. Sarkar, H. P. van der Meulen, J. M. Calleja, J. M. Meyer, R. J. Haug, and K. Pierz, "Piezoelectric exciton acoustic-phonon coupling in single quantum dots," Phys. Rev. B **78**, 241305(R) (2008).
32. G. Moody, M. E. Siemens, A. D. Bristow, X. Dai, D. Karaiskaj, A. S. Bracker, D. Gammon, and S. T. Cundiff, "Exciton-exciton and exciton-phonon interactions in an interfacial GaAs quantum dot ensemble," Phys. Rev. B **83**, 115324 (2011).
33. J. Bylsma, P. Dey, J. Paul, S. Hoogland, E. H. Sargent, J. M. Luther, M. C. Beard, and D. Karaiskaj, "Quantum beats due to excitonic ground-state splitting in colloidal quantum dots," Phys. Rev. B **86**, 125322 (2012).
34. E. Harel, S. M. Rupich, R. D. Schaller, D. V. Talapin, and G. S. Engel, "Measurement of electronic splitting in PbS quantum dots by two-dimensional nonlinear spectroscopy," Phys. Rev. B **86**, 075412 (2012).

1. Introduction

Semiconductor quantum dots (QDs) are promising candidates for a number of optoelectronic applications, including lasers, photovoltaic devices, and photon detectors [1]. The optical properties of InAs QDs strongly depend on the embedded matrix of the quantum dots [2,3]. Substantial efforts have been made to develop a GaAs-based 1.3-μm InAs QD lasers for optical-fiber telecommunication with advantages of low threshold current density, high thermal stability, and rapid bandwidth modulation [4–6]. The InAs QD lasers operated at excited state (ES) was shown to be superior to that with ground-state (GS) operation because of the advantages of high saturation gain, reduced carrier scattering time, and large modulation bandwidth [7, 8]. However, extending the QD emission wavelength remains a challenge owing to the degraded optical properties of InAs/GaAs QD heterostructures [9, 10]. Thus, it is crucial to advance our knowledge of the dynamics of optically excited InAs quantum dots (QDs). We developed an interrogative technique to directly probe into the ultrafast optical response of InAs QDs based on adaptive control of light-matter interaction.

#222441 - $15.00 USD Received 3 Sep 2014; revised 29 Oct 2014; accepted 21 Nov 2014; published 4 Dec 2014

The ability to control the time evolution of a quantum system is of fundamental importance to quantum technology [11]. Coherent control had been realized with femtosecond laser pulse shapers based on spatial light modulators (SLM) [12]. Adaptive coherent control can yield dynamic information of a quantum system by interrogating it without *a priori* knowledge of its Hamiltonian [13]. Several feasible ways had been demonstrated to achieve the goal of adaptive quantum control [14–16]. In the adaptive quantum control with femtosecond pulse shaper, phase-only shaping affects the time ordering of the constituent frequencies in a given pulse without changing the fundamental spectrum of the laser pulse [17]. Thus, the only way to encode information into the phase of a laser pulse is via coherently manipulable processes.

Current study with femtosecond coherent control technique aims not only to control the evolution of a complex system but also to deduce the underlying dynamic mechanism from the optimal laser field [17]. To further advance the field, it is important to derive the physical meaning of an adaptive control from the characterization of a systems response. In this regard, a variety of spectroscopic techniques is valuable to verify the controllability and to interrogate control mechanisms [18].

Two-dimensional coherent spectroscopy (2D CS) had been demonstrated to be a valuable tool to probe a quantum system with simultaneously high spectral and high temporal resolution [19]. Many-body interactions among semiconductor excitons produce distinct features in two-dimensional coherent spectra [20, 21]. A measured variation of the dephasing rate of excitons can reveal high-order correlations [22]. By using different polarizations or spectrally shaped pulses [23,24], it is possible to isolate specific quantum coherent pathway and distinguish cross coupling between spatially separated with 2D CS [24].

In this study, we investigated the dynamics of excitons at excited state in InAs QDs embedded in two different types of strain-reducing layers (SRL). We probed the InAs QDs at 1.2 μm with a two-photon excitation spectroscopy using phase-only shaping technique. By adaptively control the light matter interaction, a delayed resonant response from the InAs QDs was found to be encoded in the optimal phase profile of ultrafast optical pulse used. We verified the delayed resonant response to originate from excitons coupled to acoustic phonons of InAs QDs with two-dimensional coherent spectroscopy. Our approach may be useful to provoke further study of the optical excitation and coupling processes of quantum confined structures and to understand how the optical excitation delocalizes over the whole structure.

2. Experimental methods

2.1. Freezing phase algorithm for adaptive coherent control

We first illustrate the principle of the freezing phase algorithm (FPA) [25, 26] to be used for ccTPF. Figure 1(a) shows a phase-distorted coherent pulse on the complex field plane, assuming the pulse to have four spectral components: $E(t) = \sum_{n=1}^{n=4} \nu_n(t) e^{i\phi_n(t)}$. To freeze the spectral phases, we first pick up a component, for example, $\nu_4 e^{i\phi_4}$ and align it to the combined direction of the rest three components [see Fig. 1(b)]. The same procedure is repeated for $\nu_3 e^{i\phi_3}$, $\nu_2 e^{i\phi_2}$, and $\nu_1 e^{i\phi_1}$ until a frozen state is reached [Fig. 1(f)].

2.2. Optical apparatus

The adaptive pulse shaping apparatus used in this study comprises a CW mode-locked Cr^{4+}:forsterite laser. The output of the laser was 280 mW with a central wavelength of 1.253 μm at a repetition rate of 76 MHz. The full-width-at-half maximum (FWHM) bandwidth was 42 nm, corresponding to 50-fs pulse duration. Two-photon excitation fluorescence spectrum was acquired with a spectrograph equipped with a cooled CCD camera. An integrated spectrum over a specific wavelength range was feedback to control the phase retardation pattern of a liquid crystal SLM in a 4-f pulse shaping system [25].

#222441 - $15.00 USD Received 3 Sep 2014; revised 29 Oct 2014; accepted 21 Nov 2014; published 4 Dec 2014

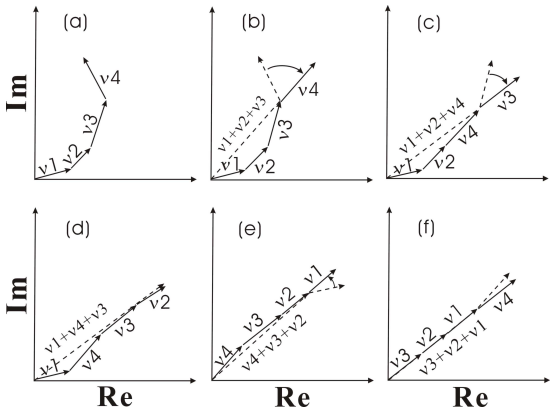

Fig. 1. Schematic diagrams showing successive freezing steps of a phase-distorted coherent pulse [25,26]. For simplicity, the spectral phase profile of the pulse is represented with four components only.

Our near infrared 2D CS was built on an amplified femtosecond laser system tunable from 1.1 to 1.8 μm at a repetition rate of 1 kHz. As depicted in Fig. 2(a), the laser output was split into four parts. Each part has a pulse energy about 60 nJ/pulse. Three of the four beams were focused into the sample under study in a boxcar phase matching geometry. The pulses right in front of the sample were analyzed with frequency-resolved optical gating (FROG) technique. The result was presented in Fig. 2(b), showing a FWHM duration of 125 fs. The diameter of the focused spots was about 50μm, which encompassed an ensemble of 2×10^5 InAs QDs. An initial state of the sample is prepared by exciting the sample with the first two pulses arriving at times t_1 and t_2, which define the coherence time interval t=t_2-t_1. The time interval between the second and third pulses, called the waiting time T=t_3-t_2. Varying the delay time T allows insight into the dissipative population dynamics within the excitation manifold. Finally at the instant of t_3, the resulting quantum state was probed with the third pulse to generate new coherences that emit an echo in the phase-matched direction $\vec{k}_s=\vec{k}_2-\vec{k}_1+\vec{k}_3$. The fourth beam was attenuated by a factor of 1000 and used as a local oscillator (LO) for heterodyne detection of the echo field. The interferogram was recorded as the delay t was increased mechanically with a step size of 3.3 fs, while the delay T was held fixed.

The excitation axis of a 2D spectrum was constructed by taking a Fourier transform with respect to t, while the emission axis was generated by resolving the complex field spectrum with spectral interferometry. The excitation axis was plotted as negative because the conjugate pulse was incident on the sample first. The resulting 2D spectrum links the dipole oscillation frequency during the initial dephasing period with that of the final rephasing period for each waiting time T [19]. The shapes of peaks appearing on the diagonal provide a measure of the memory of the system, while cross-peaks provide information on electronic coupling.

2.3. Device fabrication

The schematic of the device structure and the associated energy level diagram were described in Fig. 3(a). The fabrication process started with a 300 nm-thick GaAs buffer layer on a semi-insulating GaAs (100)-oriented substrate. A monolayer of InAs QDs with 1×10^{10} QDs/cm^2 was grown at 530°C in Stranski-Krastanov growth mode with a Riber32P molecular beam epitaxy system [2,3]. The QDs were covered with a 6 nm-thick SRL to increase the confinement potential, reduce the compressive strain in InAs QDs, and suppress the indium segregation.

#222441 - $15.00 USD Received 3 Sep 2014; revised 29 Oct 2014; accepted 21 Nov 2014; published 4 Dec 2014

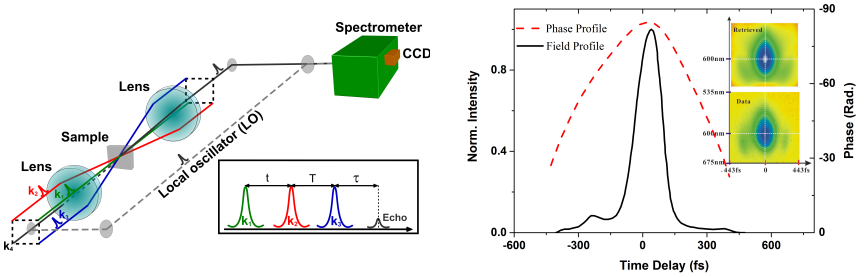

(a) (b)

Fig. 2. (a) Schematic showing the two-dimensional coherent spectroscopy with four phase-stabilized pulses propagating to the sample in a boxcar phase matching geometry. The timing diagram of the three excitation pulses and the echo pulse was depicted on the right side. (b) Retrieved field (solid curve) and phase (dashed curve) profiles of 1.2-μm pulse measured at a position right in front of the sample under study. Inset: the measured and retrieved FROG patterns.

Finally, the samples were capped with a 100 nm-thick GaAs overlayer.

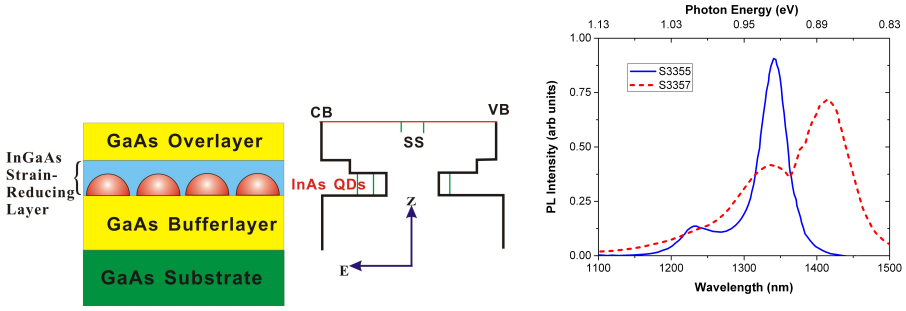

(a) (b)

Fig. 3. (a) Schematic diagrams showing the device structure and its energy level diagram. (b)One-photon excitation photoluminescence spectrum of InAs QD devices with different types of strain-reducing layers ($In_{0.18}Ga_{0.82}As$: blue solid curve; $In_{0.18}Ga_{0.82}As_{0.8}Sb_{0.2}$: red dashed curve).

2.4. Photoluminescence characterization

Figure 3(b) presents the one-photon excitation photoluminescence (PL) spectra from the InAs QD devices with different types of SRLs (S3355: $In_{0.18}Ga_{0.82}As$ (blue solid line); S3357: $In_{0.18}Ga_{0.82}As_{0.8}Sb_{0.2}$) (red dashed curve)). The PL was excited by a solid-state laser of wavelength 532nm with an excitation power of 50 W/cm^2. The PL spectrum of S3355 at room temperature shows a strong PL peak at 1340 nm, which is from the ground state transition. The energy separation between ground- and excited-state is about 80 meV with a FWHM linewidth of 26 meV. The narrow linewidth of InAs QDs in $In_{0.18}Ga_{0.82}As$ indicates a small variation in the InAs QD height. Incorporation of Sb element to form an $In_{0.18}Ga_{0.82}As_{0.8}Sb_{0.2}$ SRL (using a Sb flux of 1.2x10^{-6} Torr) shifts the ground-state transition PL peak down to 1420 nm. The longer emission wavelength was attributed to a reduced lattice mismatch between the InAs

#222441 - $15.00 USD Received 3 Sep 2014; revised 29 Oct 2014; accepted 21 Nov 2014; published 4 Dec 2014

QDs and the SRL. InAs QDs capped by the $In_{0.18}Ga_{0.82}As_{0.8}Sb_{0.2}$ SRL exhibit a first excited-state emission peak at 1310 nm. The energy separation decreases from 80 meV to 52 meV in accompany with an increased FWHM linewidth from 26 meV to 62 meV.

3. Results and discussion

3.1. Two-photon excitation fluorescence emission

The devices under study were excited by the Cr^{4+}:forsterite CW mode-locked laser at 1.253 μm. The resulting TPF spectrum from S3355 is shown in Fig. 4(a). The peak at 895 nm is due to the near band edge emission from the GaAs overlayer, suggesting a biaxial stress developed in the GaAs overlayer [26]. It is well established that elastic strain induced by the lattice parameter mismatch between epilayers results in significant energy bandgap shifts for IIIV alloys [27].

Above 950 nm, five peaks can be found at 965, 1000, 1030, 1060, and 1090 nm. These TPF features can be attributed to the near band edge emission from the different parts of the SRL with varying degrees of strain. Indeed, PL peaks at 940 nm, 1097 nm, and 1425 nm had been observed on an $In_{0.08}Ga_{0.92}As$/GaAs heterojunction and were attributed to from the top free surface, the internal strained layer, and the interfacial region of the heterojunction, respectively. TPF from S3357 [red dashed curve in Fig. 4(a)] exhibits similar spectral profile but 30% weaker than that of S3355, presumably due to a slight thickness variation in SRL and GaAs overlayer.

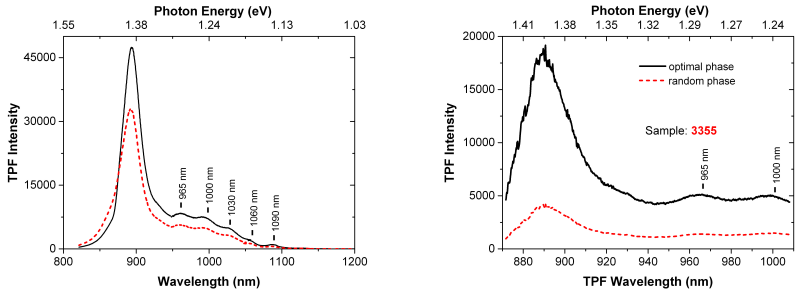

Fig. 4. (a) Two-photon excitation fluorescence spectrum of the InAs QD device with $In_{0.18}Ga_{0.82}As$ SRL (S3355: black solid line) and $In_{0.18}Ga_{0.82}As_{0.8}Sb_{0.2}$ (S3357: red dashed curve) SRL. (b) Coherent controlled two-photon excitation fluorescence spectrum of S3355 excited by 1.253 μm femtosecond laser pulse with random phase retardation profile (red dashed curve) and an optimal phase retardation profile for maximal TPF (black solid curve).

3.2. Coherent control two-photon fluorescence (ccTPF) emission

By using an adaptive pulse shaper with FPA, we can optimize the TPF signal by adjusting the spectral phase of the input femtosecond laser pulse. The measured TPF signal from 870 to 1010 nm on S3355 is presented in Fig. 4(b). The TPF spectrum (red dashed curve) was acquired with shaped pulses by imposing a random phase retardation profile on the SLM. The spectrum with black solid curve was taken with femtosecond laser pulses shaped by the optimal phase retardation profile. More than four times increase in the ccTPF signal can be achieved. In contrast to second-harmonic generation, different phase-shaped pulses always generate TPF with similar spectral profile [26], indicating that the energy relaxation processes in TPF completely remove the initial phase memory of optical excitation. Thus, by using the phase-only shaping technique, the only phase manipulable processes in ccTPF are due to the two-photon absorption (TPA).

#222441 - $15.00 USD Received 3 Sep 2014; revised 29 Oct 2014; accepted 21 Nov 2014; published 4 Dec 2014

By invoking the second-order perturbation theory, we can derive the excited-state amplitude of TPA as

$$a^{(2)}_{g\to e}(t) = \left(\frac{-i}{\hbar}\right)^2 \int_{-\infty}^{t} dt_1 \int_{-\infty}^{t_1} dt_2 \sum_m \mu_{em}\mu_{mg} E(t_1)E(t_2) e^{i\omega_{em}t_1} e^{i\omega_{mg}t_2}, \tag{1}$$

where μ_{ji} denotes the transition moment from state i to j with an associated transition frequency ω_{ji}. We can simplify the excited-state amplitude by expressing $E(t) = \int \tilde{E}(\omega) e^{-i(\omega+i\eta)t} d\omega$ and let $t \to \infty$

$$a^{(2)}_{g\to e}(t\to\infty) = \frac{-i}{\hbar^2} \sum_m \mu_{em}\mu_{mg} \int_{-\infty}^{+\infty} \frac{\tilde{E}(\omega)\tilde{E}(\omega_{eg}-\omega)}{\omega-\omega_{em}-i\eta} d\omega. \tag{2}$$

The change rate of the deposited TPA energy per unit volume can be expressed as

$$\left\langle \frac{d}{dt}(absorbed\ energy/volume) \right\rangle_t = -\frac{dI}{dz} = \beta I^2, \tag{3}$$

where β is the TPA coefficient. The TPA transition rate per unit volume $R^{TPA}_{g\to e}$ can be related to the TPA coefficient with

$$R^{TPA}_{g\to e} = \frac{\left|a^{(2)}_{g\to e}(t\to\infty)\right|^2}{\tau_p} = \frac{\beta I^2}{2\hbar\omega} \tag{4}$$

with τ_p being the pulse duration. If $\omega - \omega_{em} \neq 0$ for all m, then the TPA can be maximized by adjusting the spectral phase of excitation pulse to satisfy $\Phi(\omega_{eg}/2 - \Delta) + \Phi(\omega_{eg}/2 + \Delta) = 2n\pi,$ with $\Delta = \omega - \omega_{eg}/2$ [28]. However, if an intermediate resonant level r exists with $\omega - \omega_{er} = 0$, the integral in Eq. 2 becomes singular. In this case, we can apply Cauchys principle value technique [28] to rewrite the integral

$$\int_{-\infty}^{+\infty} \frac{\tilde{E}(\omega)\tilde{E}(\omega_{eg}-\omega)}{\omega-\omega_{er}-i\eta} d\omega = i\pi\tilde{E}(\omega_{er})\tilde{E}(\omega_{rg}) + P\int_{-\infty}^{+\infty} \frac{\tilde{E}(\omega)\tilde{E}(\omega_{eg}-\omega)}{\omega-\omega_{er}} d\omega = \tilde{R}_0 e^{-i\omega t_{lag}}, \tag{5}$$

where $\tilde{R}_0 = \sqrt{\left(\pi\tilde{E}(\omega_{er})\tilde{E}(\omega_{rg})\right)^2 + \left(P\int_{-\infty}^{+\infty} \frac{\tilde{E}(\omega)\tilde{E}(\omega_{eg}-\omega)}{\omega-\omega_{er}} d\omega\right)^2}$ and $t_{lag} = \tan^{-1}\left[\pi\tilde{E}(\omega_{er})\tilde{E}(\omega_{rg}) / P\int_{-\infty}^{+\infty} \frac{\tilde{E}(\omega)\tilde{E}(\omega_{eg}-\omega)}{\omega-\omega_{er}} d\omega\right] / \omega$. Thus, any intermediate resonant level will produce a 90^o phase shift relative to other nonresonant TPA processes.

Assuming that the spectrum of an excitation pulse has a Gaussian profile of $s_0(\omega) = \widetilde{A_0}\ e^{-\omega^2/(4\sigma^2_\omega)}$ and the spectrum of material response is narrower than that of the coherent pulse, we can express the signal spectrum from the excited material as

$$s_I(\omega) = \tilde{A_0}\tilde{R_0} e^{-\frac{\omega^2}{4\sigma^2_\omega} - i\omega t_{lag}}. \tag{6}$$

3.3. Spectral-phase sensitivity of ccTPF

We defined a spectral-phase sensitivity S(ω) to reveal how efficient does a spectral component interact with a material system [26], which gives $S(\omega) = s_0(\omega)^2 + s_0(\omega)s_I(\omega)$. The resulting sensitivity profile was Fourier transformed to the time domain

$$S(t) = \mathbb{F}\{S(\omega)\} = A_0^2 e^{-t^2\sigma^2_\omega/2} + A_0^2 R_0 e^{-(t-t_{lag})^2\sigma^2_\omega/2}. \tag{7}$$

Figure 5 presents the simulated result with Eq. 7 using $A_0 = 1$, $R_0 = 0.3$, $t_{lag} = 300$ fs, and $\sigma_\omega = 0.01$. Clearly, the main peak reflects the autocorrelation of the coherent pulse used and

#222441 - $15.00 USD Received 3 Sep 2014; revised 29 Oct 2014; accepted 21 Nov 2014; published 4 Dec 2014

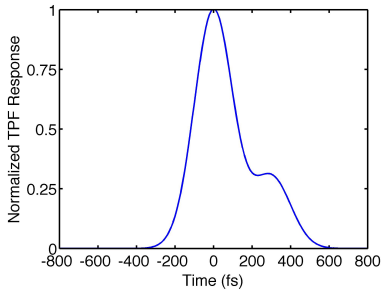

Fig. 5. Simulated result with Eq. 7 using $A_0 = 1$, $R_0 = 0.3$, $t_{lag} = 300$ fs, and $\sigma_\omega = 0.01$.

the shoulder at 300 fs originates from the material's response with a given resonance-induced time lag.

Experimentally, we can measure the spectral-phase sensitivity at a chosen component by calculating the difference of the maximal and the minimal signal as the spectral phase of the component is varied from 0 to 2π. We repeat the measurement across the entire spectrum of the coherent pulse [26]. Figure 6(a) presents the spectral-phase sensitivity profile of ccTPF and the optimal phase retardation pattern for S3355. Several peaks and valleys were observed, which were attributed to multiple TPA processes with different phases involved in the ccTPF measurement. In contrast, we obtained a smoother sensitivity profile with S3357 [see Fig. 6(b)]. This can be understood in viewing that the incorporation of Sb element in SRL alters the band offset and therefore the potential barrier to InAs QDs [3]. As shown in Fig. 3(b), the quaternary $In_{0.18}Ga_{0.82}As_{0.8}Sb_{0.2}$ SRL in S3357 shifts the transition energy of InAs QDs to outside the excitation pulse spectrum, thus effectively removes the resonance with intermediate levels.

$S(\omega)$ and the optimal phase pattern $\Phi(\omega)$ carry the complete interaction information of light field with a device. We compensated the phase distortion $\Phi_{3357}(\omega)$ of S3357 with SLM for $\Delta\Phi_{3357}(\omega) = \Phi_{3357}(\omega) - \Phi_{SLM}(\omega) = 0$. The red dashed curve in Fig. 6(c) shows the Fourier transform of $S_{3357}(\omega)e^{i\Delta\Phi_{3357}(\omega)}$. The TPF response function is dominated by the autocorrelation of the laser pulse. The blue solid curve shows the TPF response of S3355, which is given by the Fourier transform of $S_{3355}(\omega)e^{i[\Phi_{3355}(\omega)-\Phi_{3357}(\omega)]}$. Because the excited state resonance of InAs QDs lies on the high frequency side of the laser spectrum, the response profile is not symmetric. It is interesting to find that except the autocorrelation peak of the laser pulse the TPF response of S3355 peaks at 260 fs and 650 fs. Since all other TPF contributions had been properly compensated, these response peaks shall be attributed to from the resonances with excitons in InAs QDs. We shall also emphasize that although only coherently manipulable processes are involved in TPA, our CCD camera can pick up TPF signals even when the excitation pulse disappears. Thus a wider range of dynamics can be probed with adaptive coherent control, which may be advantageous for the interrogative technique demonstrated here.

3.4. 2D CS study at different waiting times

We applied 2D CS to decipher the underlying process of the ccTPF responses shown in Fig. 6(c). The measurement was executed by exciting S3355 with three phase-stabilized coherent pulses at λ_0=1.2μm [see Fig. 2]. The spectrum of the ultrashort pulses overlaps with the first excited level of InAs QDs. The emitted photon echo field was Fourier transformed over the coherent time t. The magnitudes of the 2D spectra measured at four different waiting times, T=0 fs, 33 fs, 67 fs, 100 fs, and 234 fs, are presented in Fig. 7.

Owing to the rephasing process of 2D CS, two closely neighboring peaks at (249 THz, -249

#222441 - $15.00 USD Received 3 Sep 2014; revised 29 Oct 2014; accepted 21 Nov 2014; published 4 Dec 2014

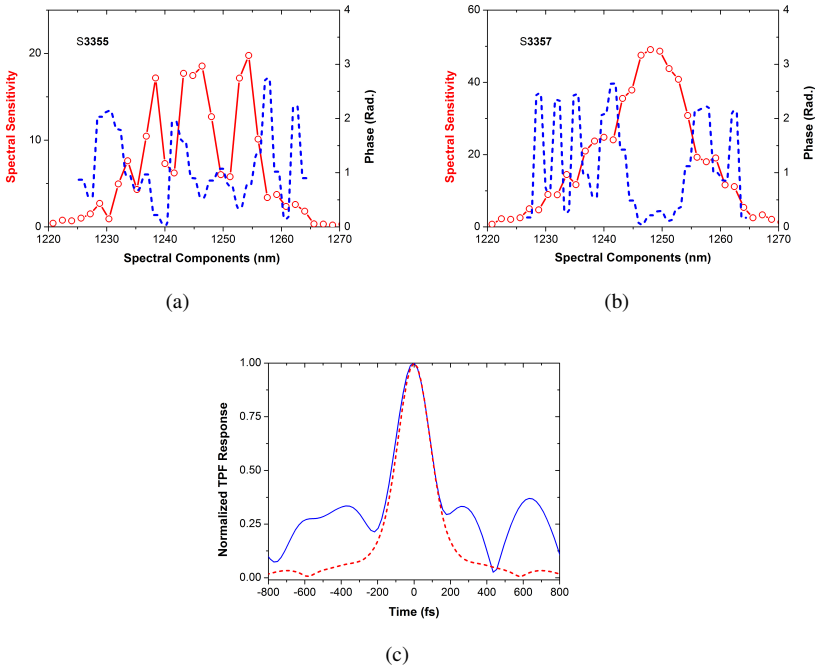

Fig. 6. Spectral-phase sensitivity curves of ccTPF and the spectral-phase patterns used to generate maximum ccTPF signal from the InAs quantum dot device with (a) $In_{0.18}Ga_{0.82}As$, (b) $In_{0.18}Ga_{0.82}As_{0.8}Sb_{0.2}$ strain-reducing layer . (c) Fourier transform of the spectral-phase sensitivity profiles shown in (a) blue solid curve and (b) red dashed curve.

THz) and (251 THz,-252 THz) can still be resolved in the 2D spectra. The main peak at (249, -249) persists up to T=234 fs without changes its position and shape. However, the peak at (251, -252) decays rapidly and shifts to (251, -251) at T=67 fs accompanied the presence of a cross peak at (251, -249), indicative of a coupling with the main peak at (249, -249). The coupling damps out at T=234 fs, leading to disappearance of the cross peak and recovery of (251, -252) peak.

The frequency difference between the two diagonal peaks is about 2-3 THz, corresponding to 67-100 cm^{-1} frequency splitting. The frequency splitting is about a factor of 2.5 lower than the calculated value of TO and LO modes in an InAs QD [29]. However, it is known that InAs possesses a nonvanishing piezoelectric effect ($\partial Q/\partial E \neq 0$). The ultrashort optical pulses E used in ccTPF and 2D CS can generate a lattice distortion Q accompanied with exciton generation in InAs QDs [30,31]. The resulting exciton-acoustic phonon coupling can contribute to the 2D CS signal by modulating the third-order nonlinear optical susceptibility $\Delta\chi^{(3)} = \left(\partial\chi^{(3)}/\partial Q\right)_{Q=0} \cdot (\partial Q/\partial E)$. The modulation of InAs unit cell by acoustic phonon is phase sensitive. As the exciton generated encounters a compressed unit cell, the exciton binding may become stronger, which may cause the anti-Stokes process to dominate the 2D CS signal. The appearance of the cross peak at one side of the diagonal line indicates that the coherent coupling process receives energy from the InAs lattice. Thus, we believe that the observed cross peak shall reflect the presence of exciton-acoustic phonon coupling in InAs QDs. The amplitude of the cross peak is relevant to the built up dynamics of acoustic phonon mode, which could last

#222441 - $15.00 USD Received 3 Sep 2014; revised 29 Oct 2014; accepted 21 Nov 2014; published 4 Dec 2014

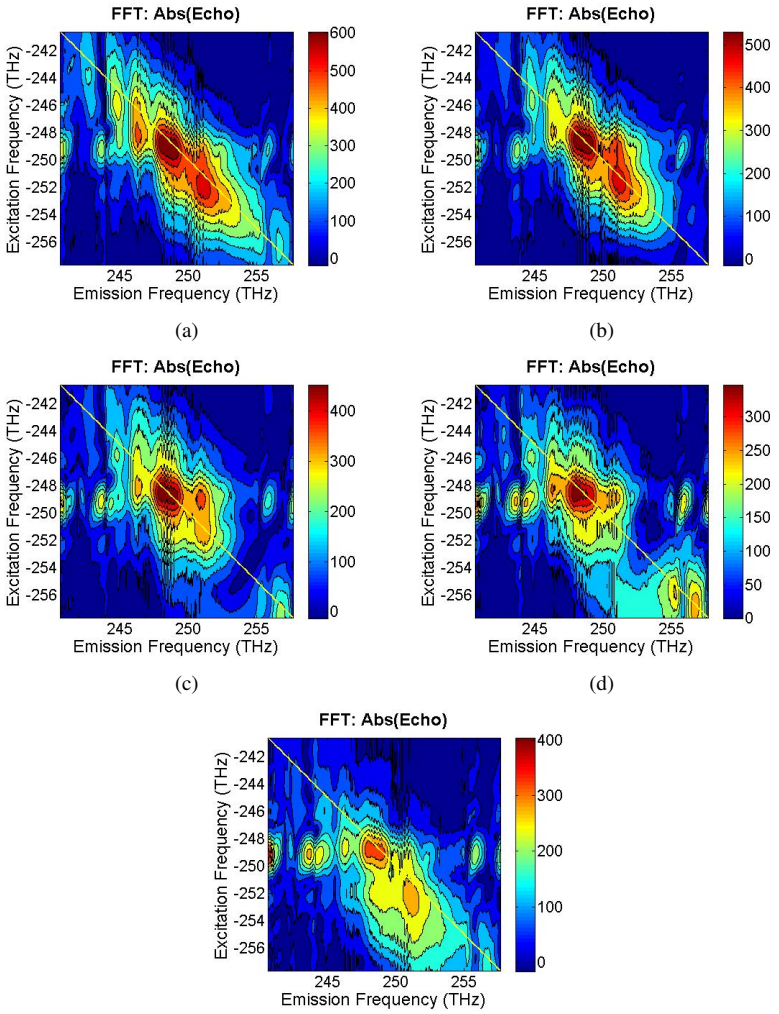

Fig. 7. 2D coherent spectroscopy of the InAs QDs device with an $In_{0.18}Ga_{0.82}As$ strain-reducing layer. The device was excited by three ultrashort laser pulses with a spectrum covering from 1164 nm (258 THz) to 1246 nm (240 THz). During the 2D CS measurements, the waiting time was fixed at (a) 0 fs, (b) 33 fs, (c) 67 fs, (d) 100 fs, and (e) 234 fs. Note 249 THz=1029.8 meV=1203.4 nm, 251 THz=1038.1 meV=1194.4 nm, 252 THz=1042.2 meV=1189.7 nm, respectively

#222441 - $15.00 USD Received 3 Sep 2014; revised 29 Oct 2014; accepted 21 Nov 2014; published 4 Dec 2014

for several hundred femtoseconds and be pick up by ccTPF as shown in Fig. 6(c). However, the relaxation of exciton population in InAs QDs is much faster, which prevents 2D CS spectra to be observed at $T > 234$ fs.

As a final remark, exciton-phonon coupling in semiconductor nanostructures had also been observed previously with 2D CS. For example, Moody, *et al*. investigated an ensemble of interfacial GaAs quantum dots with 2D CS and found that elastic scattering of excitons with acoustic phonons contributes significantly to the observed thermal broadening of the homogeneous linewidth of excitons [32]. Bylsma, *et al*. also discovered that the dephasing rate of excitons in colloidal PbS quantum dots was accelerated by the scattering of acoustic phonon [33]. At low exciton occupancy, electronic coupling between nearly degenerate exciton states of PbS quantum dot can occur due to phonon-assisted transitions [34]. 2D CS simultaneously offers both high spectral resolution and high temporal resolution and becomes a unique tool to reveal such ultrafast coherent coupling phenomena.

4. Conclusion

InAs QDs devices with different types of strain-reducing layers had been fabricated and analyzed to demonstrate the effectiveness of the strain-reducing layers. By combining one-photon and two-photon excitation fluorescence spectroscopies, varying degrees of strain were revealed in the $In_{0.18}Ga_{0.82}As$ layer. Incorporation of Sb into the SRL effectively red shifts the ground and excited state transition energies of excitons in InAs QDs. We developed an adaptive control scheme of light matter interaction to directly probe into the ultrafast optical response of InAs QDs. The coherent control TPF of the devices exhibits a resonance-induced time lag response at 260 fs and 650 fs. We further employed 2D CS to decipher the resonant response and found it to originate from an exciton-acoustic phonon coupling in InAs QDs. The dynamical information is valuable to provoke further study of the optical excitation and coupling processes of quantum confined structures.

Acknowledgments

JYH thank the National Science Council of the Republic of China for its financial support under grant number NSC100-2112-M-009-015-MY3.

#222441 - $15.00 USD Received 3 Sep 2014; revised 29 Oct 2014; accepted 21 Nov 2014; published 4 Dec 2014